First Experimental SCAN/MTI Results Achieved With the Multi-Channel SAR-System PAMIR

Delphine Cerutti-Maori, Ursula Skupin
FGAN - Forschungsinstitut für Hochfrequenzphysik und Radartechnik (FHR)
Neuenahrer Str. 20, D-53343 Wachtberg, Germany
Tel: +49 228 9435-290, Fax: +49 228 9435-618, E-mail: cerutti@fgan.de

Abstract

The airborne experimental SAR system PAMIR has been conceived by FGAN-FHR in order to demonstrate some features of future reconnaissance systems. Since 2003, the new SCAN/MTI mode has been implemented and experimentally tested. This mode provides a significant improvement to the usual MTI mode with fixed beam, since the antenna is regularly steered to different azimuth angles, allowing to scan much larger scenes. Some specific algorithms are currently under development in order to process the SCAN/MTI data gathered during the flight campaign of November 2003. This paper presents the first SCAN/MTI results achieved with the PAMIR system.
After a description of PAMIR, the flight experiment is outlined. Then an overview of the SCAN/MTI signal processing is given. Finally some first results are shown.

1 Introduction

The airborne experimental SAR system PAMIR has been designed to fulfil the increasing requirements for future reconnaissance systems and to demonstrate the possibilities of such systems. The PAMIR system is equipped with a multi-channel active phased array, which provides high flexibility and multi-mode operation such as SAR imaging (stripmap, sliding, spotlight, IfSAR and bistatic modes), ISAR imaging and MTI. The system currently operates with 3 parallel receiving channels and will possess 5 channels in its final realization stage. The most important design parameters of PAMIR in the actual development phase are listed in **Table 1**. A detailed description of PAMIR is given in [1] and [2].

One important application of PAMIR is the detection, velocity estimation and positioning of moving targets. This task is achieved via multi-channel signal processing algorithms such as STAP (Space-Time Adaptive Processing) (see [3]). A relevant mode is the SCAN/MTI mode, which allows to detect moving targets rapidly in a wide area: In order to illuminate a larger ground surface than in a usual fixed squint mode, the antenna is steered to another azimuth angle after each burst and therefore successively scans different portions of the ground. **Fig. 1** illustrates this operation. Moreover, the PAMIR system has a total bandwidth of 1.8 GHz, which is separated into 5 subbands. To increase the detection performance (the blind velocities are different for each frequency band), a sequence of pulses is sent in each frequency band successively for each look direction. In order to adapt the range resolution to the target dimension and to cover a larger swath, the instantaneous bandwidth can be reduced to 25 MHz.

This special SCAN/MTI mode is implemented in the PAMIR system and has been experimentally tested. Some specific algorithms are currently being developed at FGAN-FHR in order to process the recorded data. This paper presents the first SCAN/MTI experimental results. After a presentation of the experiment, the processing algorithm is described and some first results are shown.

Center frequency	9.45 GHz
Bandwidth	1800 MHz
Antenna	sector horn array (40 elements and 40 T/R modules) electronically steerable
Transmit power	200 W peak
Range	$>$ 30 km
Channels	3 parallel receiving arrays
Azimuth scan angle	$\pm$ 45 degrees
Azimuth beam width	2.8 degrees
Elevation steering	mechanically
Elevation beam width	12.5 degrees
Polarisation	HH
Moving target sensitivity	$\leq$ 1 m/s

Table 1: Basic system parameters of PAMIR (November 2003)

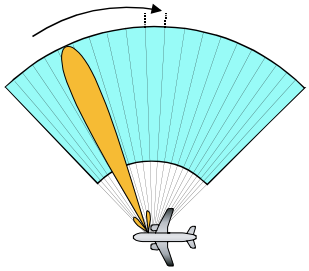

Figure 1: SCAN/MTI Mode

2 Experiment

During the flight campaign of November 2003, SCAN/MTI data were obtained with the PAMIR sensor. The preparation of the experiment and the choice of the scene were carried out in order to acquire data which are of particular interest for tracking. The experimental system carried by a Transall C-160 flew for approximately half an hour in an octagonal course and illuminated a scene of 6 km $\times$ 9 km in which both civilian and military vehicles were moving according to a planned scenario. The vehicles were divided into three different groups and some of them were equipped with GPS. Some of the instructions were to drive with varying velocities, to stop and to pass the other groups. A SAR image of the scene is shown in **Fig. 2**.

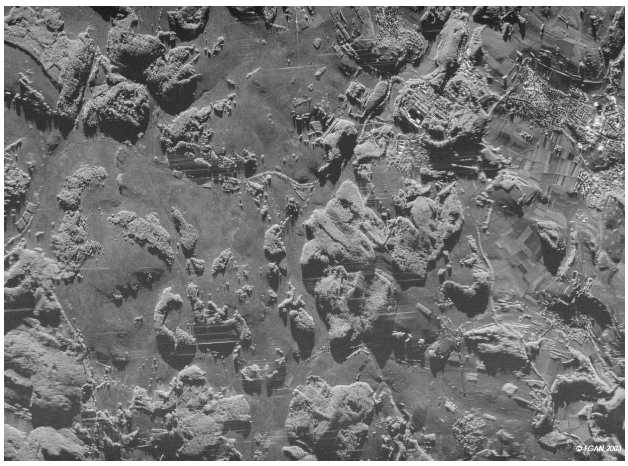

Figure 2: SAR image of the experiment region

3 MTI Processing

The processing of the SCAN/MTI raw data is performed independently for each look direction of each scan sequence. The data of the five frequency bands are first processed separately and afterwards combined incoherently. The processing scheme is the same for all look directions, which allows to compute the data in parallel, and can be separated into three main parts: clutter cancellation, detection of the moving targets and determination of their position. The following sections give an overview of the data processing. The whole SCAN/MTI processing algorithm is summarized in **Fig. 3**.

3.1 Clutter suppression

The clutter suppression filter is based on the eigenspace projection in the Doppler domain (see [4]). Since a long sequence of azimuth pulses is regarded, the contributions of the random variables in different frequency cells are considered to be asymptotically decoupled.

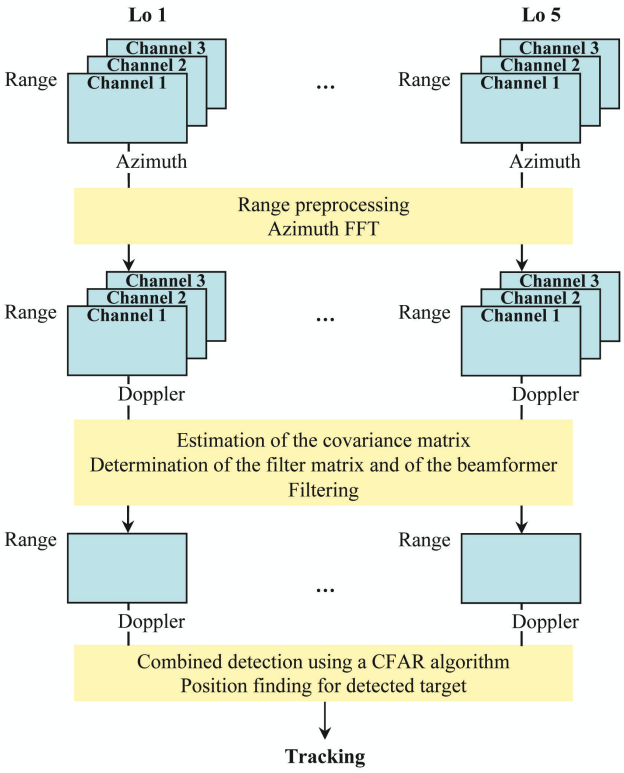

Figure 3: SCAN/MTI processing chain for each scan direction

Because of the varying flight parameters, the clutter has to be cancelled adaptively, i.e. the clutter-plus-noise spectral density matrix has to be estimated and can't be assumed to be known. Due to the antenna geometry (side-looking array configuration with identical elevation characteristics), the empirical spectral density matrix is calculated for each Doppler frequency by averaging along the range bins

$$\mathbf{R}(f) = \frac{1}{R}\sum_{r=1}^{R}\mathbf{Z}(r,f)\mathbf{Z}(r,f)^{*} \qquad (1)$$

where $\mathbf{Z}(r,f)$ denotes the receive signal vector for all the arrays at range r and Doppler frequency f after a range preprocessing including channel calibration and range compression. Since a large number of range bins is available, the variance of the estimated matrix is low.

A fundamental property of the clutter is that it is defined in optimum conditions (Nyquist sampling...) by a one-dimensional subspace, the clutter subspace, which is spanned by the DOA vector. The clutter-plus-noise spectral density matrix can therefore be approximated by

$$\mathbf{R}(f) \approx \gamma(f)\mathbf{d}(\mathbf{u}(f))\mathbf{d}(\mathbf{u}(f))^{*} + \sigma^{2}\mathbf{I} \qquad (2)$$

with $\mathbf{d}(\mathbf{u}(f))$ the DOA vector for the direction $\mathbf{u}(f)$ from which the Doppler frequency f is expected, σ the noise variance and $\gamma(f)$ a complex constant.

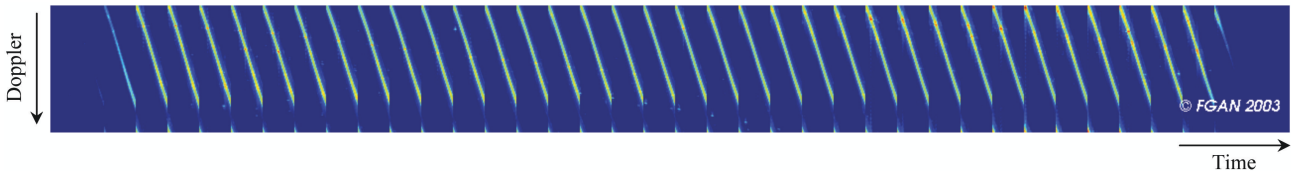

Figure 4: Doppler over time (first frequency band, second receive array)

As a consequence, the clutter can be removed by projection on a subspace orthogonal to the clutter subspace. The clutter filter matrix $\mathbf{P}(f)$ based on the eigenvector subspace projection is given by

$$\mathbf{P}(f) = \mathbf{I} - \mathbf{v}(f)\mathbf{v}(f)^* \tag{3}$$

where $\mathbf{v}(f)$ denotes the eigenvector of the largest eigenvalue of $\mathbf{R}(f)$. This filter has the advantage of really cancelling the clutter up to the noise level.
From the clutter-Doppler centroid, the scan direction $\mathbf{u}_s$ is estimated. The beamformer for that look direction is multiplied with the projector $\mathbf{P}(f)$ to obtain the whole filter vector. This filter is then applied to the data as follows

$$Z^{(f)}(r, f) = \mathbf{b}(\mathbf{u}_s)^* \mathbf{P}(f)\mathbf{Z}(r, f). \tag{4}$$

3.2 Moving target detection

After clutter suppression and coherent integration is carried out for each of the frequency bands, the five resulting complex fields are co-registered and combined incoherently. This operation significantly improves target detection. Indeed, the blind velocities are varying according to the frequency band. A combination of the different bands makes therefore the detection procedure more robust.
The target detection is done via CFAR technique and is based on a threshold test. In the simplest case, the detection is performed for each range/Doppler cell independently. If the radial velocity of the target has changed considerably during the observation time, the target contribution is distributed over several range/Doppler cells, which has to be taken into account (analysis of range/Doppler trajectories). Finally the false alarms coming from strong non-moving targets are eliminated.

3.3 Position finding

The next step is to determine the position in azimuth of each detected target using monopulse or super-resolution methods such as MUSIC.
In order to get an estimate of the azimuthal position, it is necessary to return to the data before filtering and to filter for a second time the data with the clutter filter matrix $\mathbf{P}(f)$ from **Equation 4** but without the beamformer $\mathbf{b}(\mathbf{u}_s)$. Then one of the angle estimation methods can be applied.
In both cases, an accurate knowledge of the array manifold (i.e. the DOA vectors for the interesting directions) is assumed. Because of the environmental influences, a phase model or a measurement of the array manifold is not sufficient. This array manifold can be derived from the spectral density matrix in **Equation 2** because the eigenvector of the largest eigenvalue of $\mathbf{R}(f)$ constitutes an estimate of the DOA vector $\mathbf{d}(\mathbf{u}(f))$ up to a complex constant.

3.4 Output data

For each moving target, the output data include its position calculated and given in the earth reference system, its radial velocity, its current signal power, and the time of the burst in which it was detected. These data are then passed to a tracking algorithm.

4 First experimental results

The first processing test was to control if the antenna had scanned properly. For this purpose, the Doppler over time was computed for each receive array and frequency band. **Fig. 4** shows one of the processed results.
For each burst of a scan direction, the pulses received by one array were transformed into the Doppler domain and then added along the range bins. The resulting vector corresponds to the clutter-plus-targets Doppler spectrum of the data at the time of the burst. The same procedure was carried out for the other bursts. These Doppler spectra were then plotted against the burst time.
As the antenna is steered to another direction after each burst and the clutter Doppler spectrum depends on the look direction, the position of the clutter Doppler spectrum is varying according to the burst. It results in a specific pattern that recurs with each scan sequence.
Such a scan pattern could be observed for each of the processed results, which indicates an accurate scan ability of the antenna.

An important tool in order to investigate the MTI capability of a moving system is provided by the space-time characteristics. This characteristic combines the antenna characteristics with the system Doppler filter function and represents the instantaneous system sensitivity to a target at direction $\mathbf{u}$ and at Doppler f.
Fig. 5 illustrates the space-time characteristics of the first frequency band. The plotted dynamics is 50 dB. It can be seen that the MTI performance is good since a fine notch is present around the clutter direction/Doppler relationship.

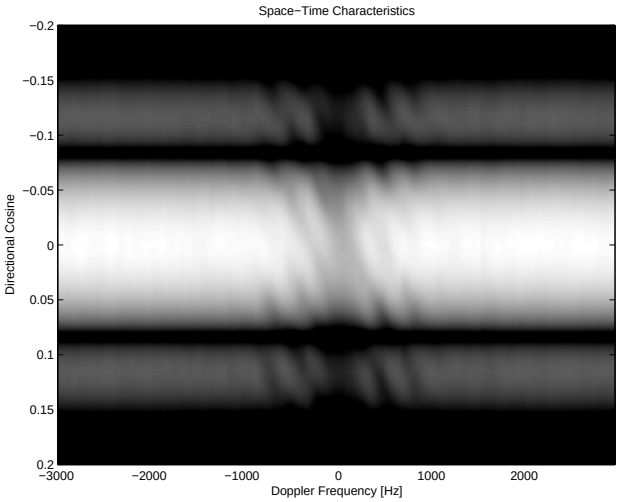

Figure 5: Space-time characteristics of the first frequency band

In order to analyse the Doppler filter efficiency, the eigenvalue distribution of the empirical spectral density was plotted. **Fig. 6** shows the eigenvalues depending on the Doppler frequency. As expected, there is a dominant eigenvalue, which represents the clutter echoes. The distance from the largest eigenvalue to the sum of the other eigenvalues is a measure how much clutter suppression can be achieved in the look direction by an eigenvector projection on the $M-1$ dimensional complement space, with M the number of receive arrays. The suppression capability here is about 25 dB.

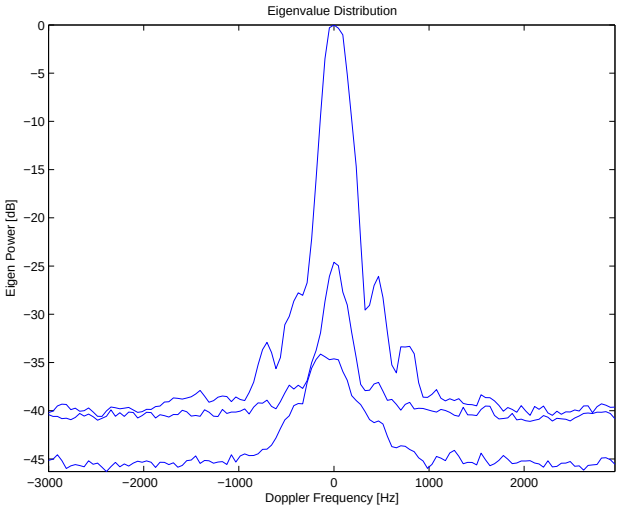

Figure 6: Eigenvalue distribution of the empirical spectral density matrix of the first frequency band

From the empirical spectral density matrix, an estimation of the array manifold can be derived since the eigenvector corresponding to the largest eigenvalue contains a measurement of the DOA vector. **Fig. 7** presents the phase of the estimated DOA vectors on the main beam clutter over the Doppler frequency.

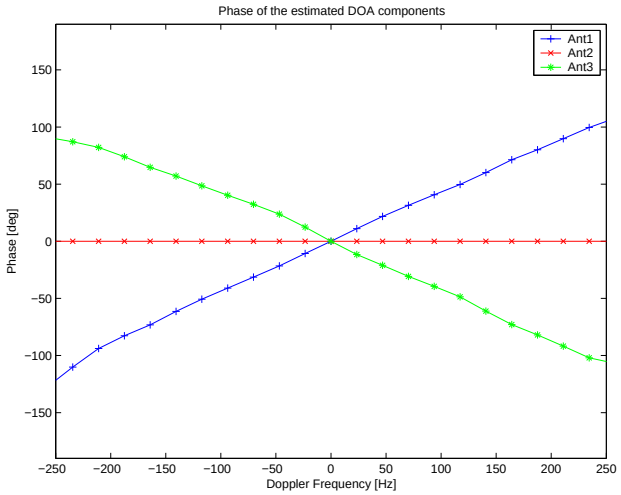

Figure 7: Measured array manifold of the first frequency band (second receive array as reference)

5 Summary

The first results obtained have proved that the SCAN/MTI experiment performed during the PAMIR flight campaign of November 2003 was successful and very promising.
Up to now, a simplified algorithm was implemented. This algorithm will be enhanced in the future and improved with supplementary features such as motion compensation, coherent subspace transformation (see [5]) and finer detection criteria.

References

[1] J.H.G. Ender, A.R. Brenner: PAMIR - a wideband phased array SAR/MTI system. IEE Proc.-Radar Sonar Navig., Vol 150, No. 3, June 2003, pp 165-172.

[2] H. Wilden, B. Poppelreuter, O.Saalmann, A. Brenner, J. Ender: Design and realisation of the PAMIR antenna frontend. EUSAR, May 2004, Ulm.

[3] R. Klemm: Principles of space-time adaptive processing. IEE, London, UK, 2002.

[4] J.H.G. Ender: Space-time processing for multichannel synthetic aperture radar. Electronics & Communication engineering journal, February 1999, pp 29-38.

[5] J.H.G. Ender: Subspace transformation techniques applied to multi-channel SAR/MTI. IGARSS, June 1999, Hamburg.